Bull Volcanol (2002) 64:254–272
DOI 10.1007/s00445-002-0202-9

RESEARCH ARTICLE

B.R. Edwards · J.K. Russell · R.G. Anderson

Subglacial, phonolitic volcanism at Hoodoo Mountain volcano, northern Canadian Cordillera

Received: 3 January 2002 / Accepted: 12 January 2002 / Published online: 14 March 2002

Abstract Hoodoo Mountain volcano (HMV) is a Quaternary phonolitic volcano situated on the north side of the Iskut River, in the Coast Mountains of northwestern British Columbia, Canada. Its activity spans the last 100,000 years, it may have erupted as recently as 9 ka, and it encompasses a volume of approximately 17 km^3. Throughout its history, much of the volcanic activity has been directly affected by glaciers, which accounts for its striking morphology and volcanic deposits. The physical development of the volcano includes at least six stages: (1) subglacial eruptions at about 85 ka; (2) ice-confined eruptions at about 80 ka; (3) subaerial(?) pyroclastic eruptions between about 80 and 54 ka; (4) subaerial effusive eruptions at about 54 ka; (5) subglacial eruptions between 54 and 30 ka; and (6) subaerial, post-glacial eruptions at about 9 ka. The chemical and mineralogical compositions of HMV lavas remained limited throughout the 100,000-year history of the HMV. All samples are phonolite or trachyte with (micro-) phenocrysts of alkali-feldspar, clinopyroxene, and magnetite. Samples are almost exclusively nepheline and acmite normative. Compared with primitive mantle values, samples from HMV are 10–100 times enriched in rare earth element concentrations and have moderate negative Eu anomalies. Field observations, petrological data sets, and thermodynamic modeling support derivation of the phonolite magmas at HMV from alkali olivine basalt by a combination of fractional crystallization and crustal assimilation at mid-crustal pressures. The attendant changes in magma density related to differentiation permitted the continued buoyant ascent and eruption of phonolitic magmas derived from basaltic parental magmas that stalled in the crust. In this environment, the slight changes in lithostatic pressure accompanying fluctuations in Cordilleran ice sheets could amplify volcanism by "glacial pumping" of the magma-charged crustal lithosphere.

Keywords Glacial volcanism · Hoodoo Mountain · Phonolite · Quaternary · Subglacial

Editorial responsibility: W. Hildreth

B.R. Edwards (✉)
Department of Geology, Grand Valley State University,
Allendale, MI 49401-9403, USA
e-mail: edwardsb@gvsu.edu

J.K. Russell
Igneous Petrology Laboratory,
Department of Earth and Ocean Sciences,
University of British Columbia, Vancouver,
BC V6T 1Z4, Canada

R.G. Anderson
Geological Survey of Canada, #101–605 Robson Street,
Vancouver, BC V6B 5J3, Canada

Introduction

The northern Cordilleran volcanic province (NCVP; Edwards and Russell 2000; Fig. 1A) is one of the largest Neogene volcanic provinces in western North America. The NCVP comprises dominantly mafic, Neogene to Quaternary, alkaline volcanic rocks thought to result from extensional forces acting on the northern Cordilleran lithosphere (Souther 1977; Edwards and Russell 1999, 2000). Three large, distinctive volcanic centers in northwestern British Columbia form the central portion of the NCVP: Mount Edziza (Souther et al. 1984; Souther 1992), Level Mountain (Hamilton 1981) and Hoodoo Mountain (Edwards 1997; Edwards et al. 2000; Fig. 1B). Relative to most other NCVP volcanoes, these are long-lived edifices comprising large volumes (>17 km^3) of intermediate to felsic alkaline lavas that do not derive directly from asthenospheric mantle sources (Hamilton 1981; Souther and Hickson 1984; Souther 1992; Edwards 1997). These three volcanoes were formerly treated as part of the Stikine volcanic belt (Souther 1977), but are now assigned to the Stikine subprovince of the NCVP (Edwards and Russell 2000).

Until recently, Hoodoo Mountain volcano (HMV) was the least studied of the large volcanic centers within the Stikine subprovince. Kerr (1948) briefly described the volcanic deposits at Hoodoo Mountain during a study

of the regional geology along the southern part of the Iskut River, and Souther (1991a) provided a short account of its striking morphology and some age-constraints from preliminary K–Ar dating. Edwards (1997) gave the first detailed summary of the Quaternary stratigraphy and petrology of the Hoodoo Mountain volcanic complex, and a detailed geologic map of the complex has recently been published (Edwards et al. 2000).

Our objectives in this paper were to examine three important components in the evolution of HMV. First, we use the field characteristics, spatial distribution, and morphology of the volcanic deposits to explore the physical evolution of HMV. Our analysis demonstrates that the physical evolution of the edifice was strongly controlled by interaction with glacial ice as thick as 2 km, resulting in the formation of ice-contact and subglacial volcanic deposits (Smellie 1999; Hickson 2000). Second, we establish the physical–chemical origins for the phonolite and trachyte magmas that fed HMV; such peralkaline magmas are most efficiently produced where alkali olivine basaltic magma stalls in the mid-crust and assimilates felsic rocks (e.g., Souther and Hickson 1984; Edwards and Russell 1998; Russell and Hauksdóttir 2000). Lastly, we use these results to explore the possible linkages between glacial loading events and the eruption of crustally stored magma (e.g., Grove 1974; Rampino et al. 1979; Sigvaldason et al. 1992; Edwards and Russell 1999). Crustal assimilation processes coupled with loading of the crust by ice can increase the potential for eruption of magma from mid-crustal depths.

Geological setting

Hoodoo Mountain volcano (56°46′N, 131°17′W; UTM center 360000E 6294500N) is situated immediately north of the Iskut River, in the Coast Mountains of northwestern British Columbia, Canada (Fig. 1C). The volcano comprises a minimum volume of 17 km^3 of fragmental and non-fragmental peralkaline volcanic rocks, including subglacial and subaerial lava flows, domes, spines, dykes, and pyroclastic deposits (Fig. 2, after Edwards et al. 2000). The development of the edifice overlaps in space and time with formation of nine small basaltic centers in the Iskut volcanic field (Fig. 1C; Stasiuk and Russell 1989; Souther 1991b; Hauksdóttir et al. 1994; Edwards 1997; Russell and Hauksdóttir 2000). One of these basaltic centers, Little Bear Mountain (volume <0.3 km^3), is located immediately north of Hoodoo Mountain (Figs. 1C, 2, and 3; Edwards 1997) and has been partly overridden by lava flows from HMV.

One of the most striking features of HMV is its geomorphic form. The volcano is circular in plan view and approximately 6 km in diameter at its base (Fig. 3B). The volcano features a rounded summit (Figs. 3A, C) at 1,850 m a.s.l., although all volcanic stratigraphy above 1,750 m a.s.l is obscured by a 3–4 km diameter icecap (Fig. 2). At present, HMV is flanked by two valley glaciers, Hoodoo glacier on the northwest and Twin glacier on the northeast (Figs. 2 and 3B).

Two sets of prominent cliffs (Figs. 3 and 4A) partly circumscribe the volcano, producing a discontinuous,

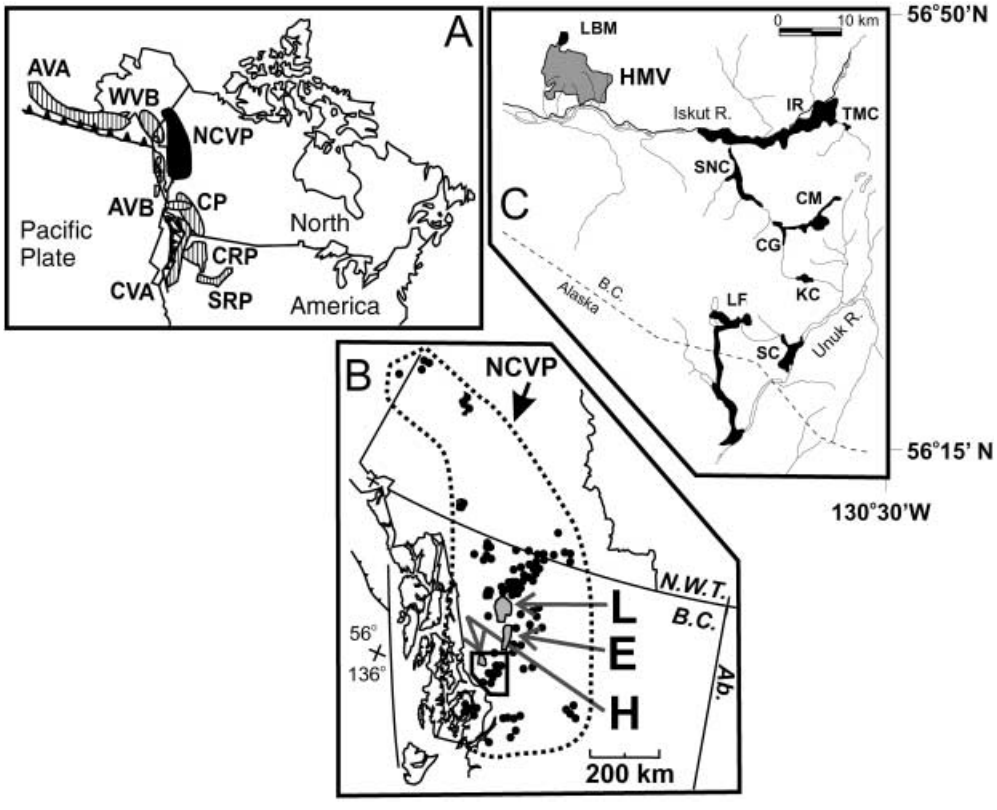

Fig. 1 **A** Location map showing the northern Cordilleran volcanic province (NCVP; Edwards and Russell 1998, 2000) and other Neogene–Quaternary volcanic provinces in western North America: *AVA* Aleutian volcanic arc, *WVB* Wrangell volcanic belt, *AVB* Anahim volcanic belt, *CP* Chilcotin plateau, *CVA* Cascade volcanic arc, *CRP* Columbia River plateau, *SRP* Snake River plain. **B** Location of Hoodoo Mountain volcano with respect to other Neogene and Quaternary volcanic centers within the NCVP including Level Mountain (*L*) and Edziza (*E*); extensively modified from Hickson (1991). **C** Map showing the location of Hoodoo Mountain volcano as well as basaltic volcanic centers in the Iskut volcanic field (Russell and Hauksdóttir 2000), including: *LBM* Little Bear Mountain, *IR* Iskut River, *TMC* Tom MacKay Creek, *SNC* Snippaker Creek, *CM* Cinder Mountain, *CG* Cone Glacier, *KC* King Creek, *LF* Lava Fork, and *SC* Second Canyon

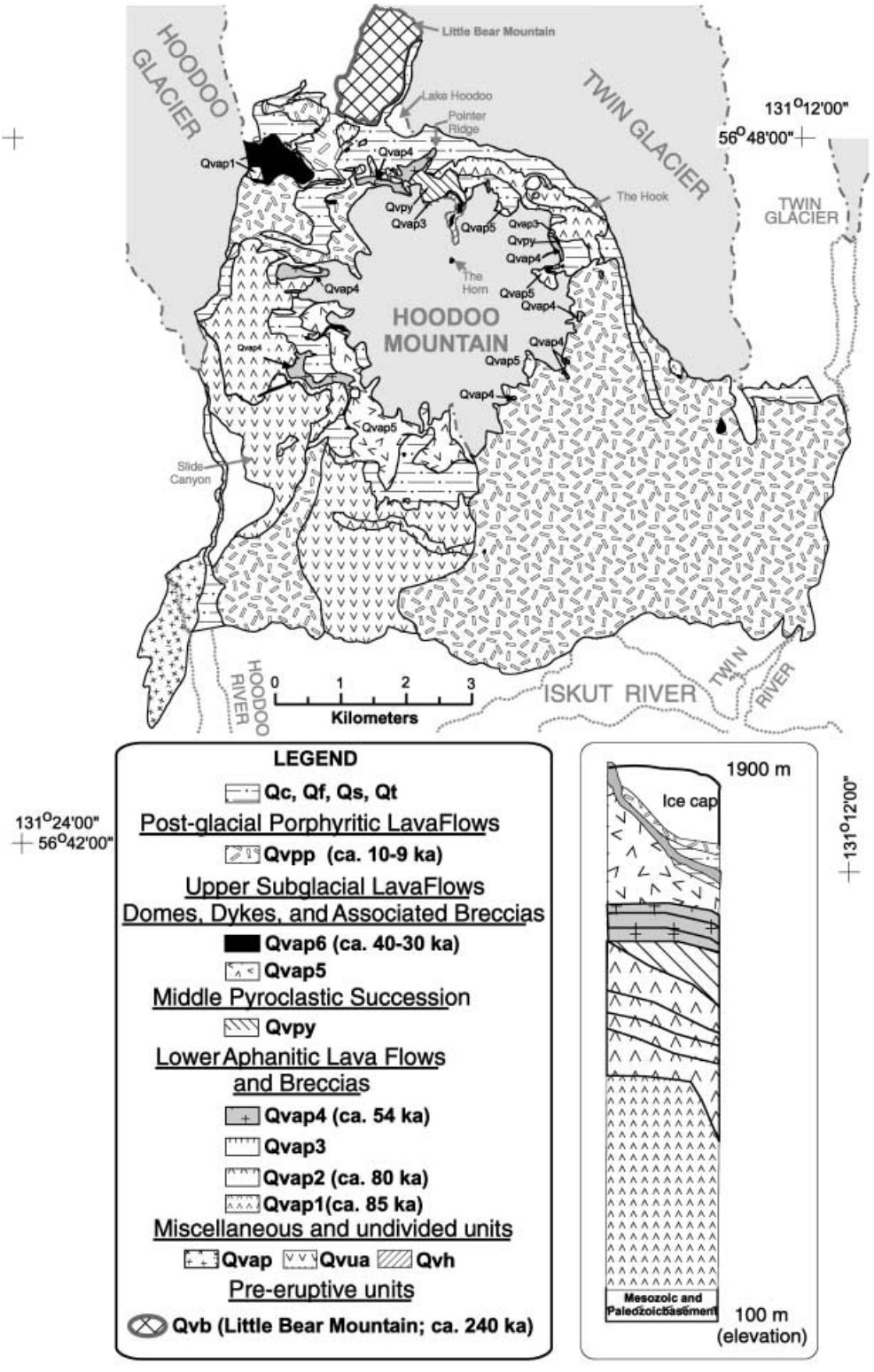

Fig. 2 Geologic map and simplified stratigraphic column for Hoodoo Mountain volcano (after Edwards et al. 2000) showing stratigraphy described in the text. $^{40}Ar/^{39}Ar$ age determinations are reported in the legend and derive from Villeneuve et al. (1998) and Edwards et al. (1999)

step-like topographic profile. The base of the volcano is delimited by a series of cliffs 100–200 m high, except on its southeastern side where the cliffs have been partly buried by the most recent lava flows. The top of the lower set of cliffs defines a broad bench at approximately 1,300 m a.s.l. (NE side of Fig. 3C), which terminates against an upper set of cliffs. The second set of vertical cliffs is between 50 and 100 m high and surrounds the summit. The striking, step-like topographic profile and bounding cliffs of HMV led Kerr (1948) and Souther (1991a) to suggest that many lava flows at HMV were obstructed or "dammed" by glacial ice.

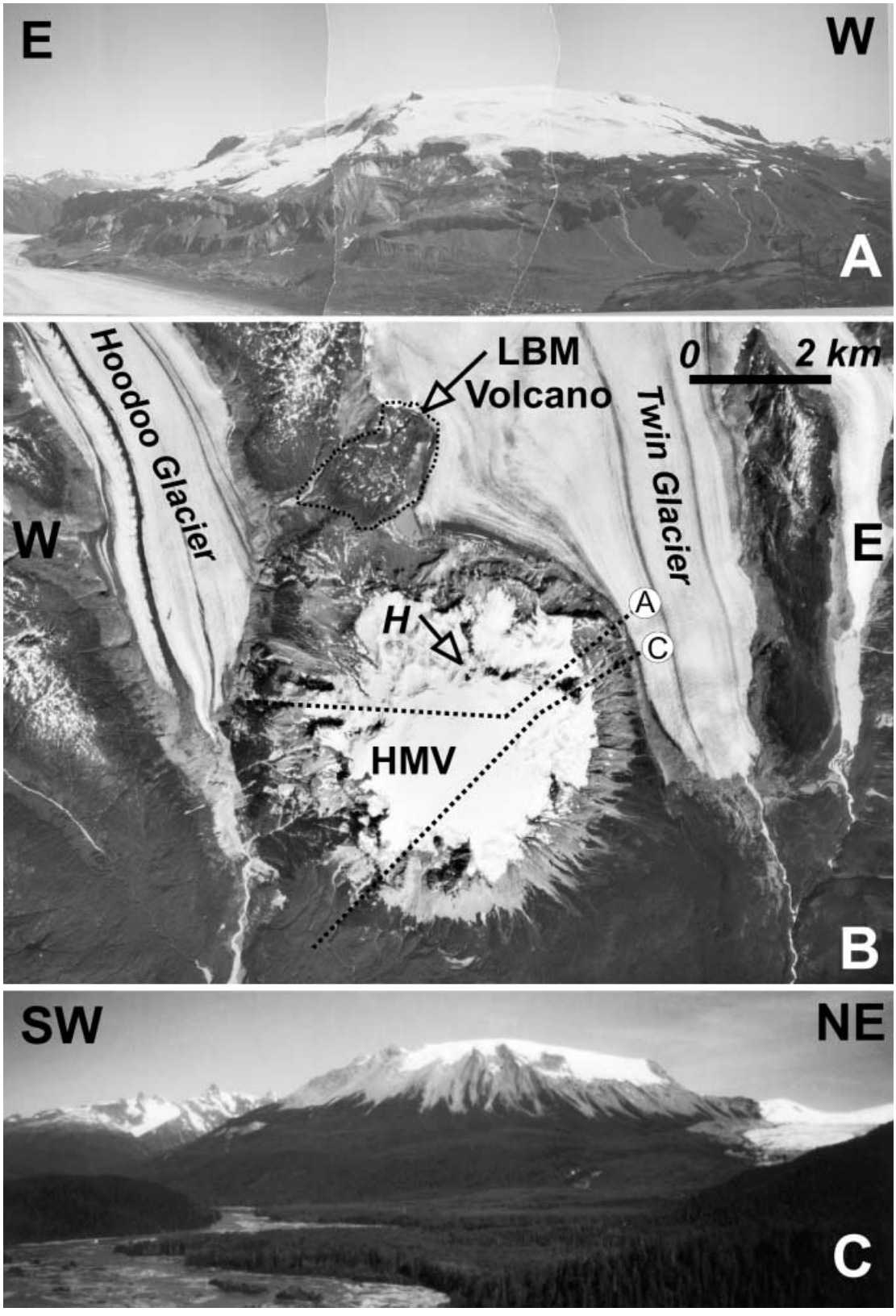

Fig. 3 **A** The north face of Hoodoo Mountain, looking south. East–west distance across the composite photograph is 5 km and vertical section is about 900 m. Note the prominent ice-contact cliffs on the lower eastern flanks of the volcano. **B** Plan view of Hoodoo Mountain (*HMV*), Little Bear Mountain (*LBM*) and surrounding glaciers (BC Airphoto BC82022), showing the 0.3-km^3 glacier capping the volcano (Russell et al. 1998). *Dashed lines* approximate the traces of the lines-of-section represented by the views shown in **A** and **C**. The Horn (*H*) is a prominent nunatak. **C** Looking northwest to the southeastern flank of Hoodoo Mountain, the prominent cliffs on the lower northeast flank are those seen in **A**. Vertical distance between the Iskut River (*lower left*) and the top of Hoodoo Mountain is 1,710 m

Physical evolution

The stratigraphic framework of HMV (Fig. 2), simplified from the 1:20,000 geological map of Edwards et al. (2000), provides critical constraints on the physical and chemical evolution of Hoodoo Mountain volcano. For example, several units have features consistent with eruption in an environment dominated by either water or ice or both, including massive lava enclosed within monomict breccia, over-thickened lava flows, highly irregular and fine-scale cooling joints, and glass-rich pyroclastic units interpreted as hyaloclastite. These features are similar to well-documented occurrences of subglacial/subaqueous volcanic deposits in Antarctica (e.g., Smellie and Skilling 1994; Skilling 1994; Smellie 1999), Iceland (e.g., Furnes et al. 1980; Allen et al. 1982; Werner and Schmincke 1999; Tuffen et al. 2001), and British Columbia (e.g., Mathews 1947; Allen et al. 1982; Hickson 2000). Four observations favor eruption in an ice-dominated rather than water-dominated environment: (1) much of the edifice formed at elevations 600 m above current sea level and this is above any highstand of sea level over the last 100,000 years (Smellie and Hole 1997; Tuffen et al. 2001); (2) no widespread occurrences of lacustrine deposits within the Iskut area indicative of a large standing body of water have been documented; (3) deposits of glacial till have been found interbedded with volcanic deposits; and (4) radiometric dating establishes most of the edifice to be younger than 85 ka. Several units dated at ca. 30 to 40 ka coincide with the onset of the late Wisconsinan/Fraser Glaciation in southern and central British Columbia (Stumpf et al. 2000). The detailed stratigraphic analysis of HMV presented below demonstrates not only the importance of the glacial environment of eruption, but also that the eruption environment changed significantly throughout the 85,000 years of volcanic activity at Hoodoo Mountain, producing subglacial, ice contact, and subaerial volcanic deposits.

Pre-HMV rocks (units PM, Qvb, Qt)

Paleozoic to Mesozoic metasedimentary, metavolcanic, and plutonic rocks (PM) of the Stikine terrane (Anderson 1993) underlie HMV. Pyroxene syenite comprises a significant portion of the Mesozoic basement; it outcrops along the southern margins of Hoodoo Mountain (Kerr 1948) and occurs as xenoliths in basaltic rocks of Little Bear Mountain, immediately north of HMV (Figs. 2 and 3B). The basement rocks were intruded by trachyandesite dykes at 1.8 Ma (Villeneuve et al. 1998; Edwards et al. 1999), representing the earliest known manifestations of Quaternary magmatism in the Iskut area.

Older Quaternary deposits comprise glacial till (unit Qt) and basaltic rocks from Little Bear Mountain (unit Qvb; Figs. 1C, 2, and 3B), which include massive lava, pillow lava, volcanic breccia, and hyaloclastite dated at 240 ka (Fig. 2; Edwards 1997; Villeneuve et al. 1998; Edwards et al. 1999). East of Hoodoo River, HMV lava flows directly overlie moderately consolidated glacial till. On the north side of the volcano, porphyritic HMV lava flows overlie till deposits resting on volcanic breccia of unit Qvb (Fig. 4B). All Quaternary deposits around HMV overlie Mesozoic country rocks (Fig. 4B).

HMV Stratigraphy

The stratigraphy of Hoodoo Mountain volcano comprises a diverse assemblage of volcanic rocks, dominated by units interpreted as having been erupted against or beneath glacial ice (Table 1, Fig. 2). The lower part of the edifice comprises massive, pervasively jointed lava and monomict breccia (unit $Qvap_1$; Table 1). The lava–breccia sequence is directly overlain by cliff-forming lava flows up to 200 m thick (Fig. 4A), thought to represent damming of flows against thick ice (unit $Qvap_2$; Table 1). The two lower units are overlain by up to 100 m of variably welded pyroclastic rocks (unit Qvpy; Table 1, Fig. 4C) and a thin vitrophyric lava flow (unit $Qvap_3$; Table 1) on the north-central (Fig. 4D) and western sides of the volcano (Fig. 4E). The pyroclastic rocks are directly overlain by a sequence of up to four relatively thick (10–30 m) lava flows (unit $Qvap_4$; Table 1), separated by layers of lava flow breccia and interpreted as having erupted subaerially (Fig. 4E). Units interpreted as subglacial in origin (units $Qvap_{5,6}$; Table 1) directly overlie the subaerial lava flow sequence (Fig. 4E). The lower of the two units ($Qvap_5$) comprises low vesicularity, monomict breccia (Fig. 4F) and pervasively jointed lava lobes and domes (Fig. 5A). The lava of the upper unit ($Qvap_6$) is also pervasively jointed (Fig. 5B), but the associated breccia is moderately vesicular (Fig. 5C). The stratigraphically highest lava flows (unit Qvpp; Table 1) appear to have originated near the summit of the edifice, flowed unobstructed down the flanks of HMV (Fig. 5D, E) and are interpreted to have been subaerial eruptions.

Volcano–ice interaction

The morphology of Hoodoo Mountain volcano and the character of its volcanic deposits can largely be ascribed to processes involving interaction between volcanism and glacial ice (Kerr 1948; Souther 1991a). The presence of valley glaciers currently overlying the distal portions of HMV units, as well as the summit icecap, attest to the broad importance of glaciation in the development of the local landscape surrounding HMV. However, the characteristics of volcanic units deposited throughout the entire eruptive history of the volcano indicate a more extended period of glacial-volcano interactions during the past 85,000 years.

Evidence indicative of volcano-ice interaction derives from (1) the overall morphology of some lava flows, (2) orientations and sizes of cooling joints; (3) the abundance of hyaloclastite intermixed with lavas in units

Table 1 Summary descriptions and interpretations of stratigraphic units at HMV

Unit[a]	Description	Location[b]	Age[c] (ka)	Interpretation
$Qvap_1$	Lava flows and domes interlayered with monomict breccia; aphanitic and low vesicularity with pervasive small diameter (~0.3 m) columnar joints; breccia clasts are angular, matrix- to clast-supported, similar in appearance to associated lava; total unit thickness ~500–1,000 m	Limited distribution; northwestern and southwestern flanks	85	Subglacial: subglacially erupted lava flows with hyaloclastite breccia
$Qvap_2$	Lava flows; similar to $Qvap_1$, but no associated breccia; flow thicknesses vary from ~30 to >200 m forming large cliffs; flow faces show extensive entabulature development, often with horizontally oriented columnar joints; total unit thickness ~200 m	Extensive distribution; found discontinuously around the entire base	80	Ice contact: subaerial lava flows erupted near summit of HMV (~1,300–1,400 m a.s.l.), but confined by ice at ~700 m a.s.l.; small diameter, horizontal columnar joints indicate vertical cooling surface
Qvpy	Lapilli tuff; non-welded to eutaxitic to vitrophyric; pumiceous to massive; clasts vary up to 0.3 m in diameter and are dominantly juvenile with <5% lithics; matrix-supported by yellow to light green ash; three highly welded lenses up to ~5 m thick occur in the middle of the deposit; total unit thickness ~100 m	Limited distribution; southwestern flanks	<80, >54	Subaerial: pyroclastic eruption
$Qvap_3$	Lava flow; abundant fresh and devitrified glass with heterolithic clasts up to ~5 cm in diameter; total thickness ~10 m	Limited distribution; north-central and northeast flanks	<80, >54	Subaerial: directly overlies Qvpy and is overlain by $Qvap_4$
$Qvap_4$	Lava flows; similar to $Qvap_{1,2}$ except flows lack entabulature and columnar joints are thicker (>1 m); sequence of up to five stacked lava flows separated by 1–10 m of lava breccia; total unit thickness ~200 m	Limited distribution; north-central and southwestern flanks	54	Subaerial: lava flows separated by flow top or flow bottom breccias
$Qvap_5$	Lava lobes and domes and monomict breccia; aphanitic to sparsely porphyritic (<5% phenocrysts), low vesicularity, and pervasively jointed with fine (<0.3 m) columnar joints of highly variable orientation; breccia is dominantly matrix-supported, with angular to subangular, low vesicularity clasts identical in appearance to associated massive lava; clasts range in size from 0.5 to >20 cm; matrix is orange to yellow; locally lava lobes are totally encapsulated by breccia; total unit thickness ~400 m	Extensive distribution; found discontinuously around entire summit	<54, >40	Subglacial: lava lobes and domes erupted subglacially with palagonitized (?) hyaloclastite formed by fragmentation during eruption
$Qvap_6$	Lava lobes, flows and dikes and monomict breccia; aphanitic to sparsely porphyritic (<5% phenocrysts), moderately to highly vesicular and/or amygdaloidal, pervasively jointed with irregularly oriented, fine (<0.3 m) columnar joints; breccia is varies from matrix- to clast-supported, with highly vesicular, elongated clasts up to 0.5 m long; matrix is whitish yellow; total unit thickness ~30–50 m	Moderate distribution; north-central, northwestern, western flanks	30–40	Subglacial: dike-fed lava flows erupted subglacially with palagonitized (?) to vitric hyaloclastite; columnar jointing reflects highly irregular cooling surfaces
Qvpp	Lava flows; locally blocky flow tops with channel margin levees; moderately porphyritic (15–25% phenocrysts) and locally trachytic, moderately vesicular; total unit thickness ~5–20 m	Extensive distribution; north-central, northwestern, southeastern flanks	9–28	Subaerial: no evidence for ice involvement

[a] Unit names based on the following: *Qv* Quaternary volcanic; *ap* aphanitic phonolite; *py* pyroclastic deposits; *pp* Quaternary volcanic porphyritic phonolite
[b] See Fig. 2
[c] Villeneuve et al. (1998); Edwards et al. (2000)

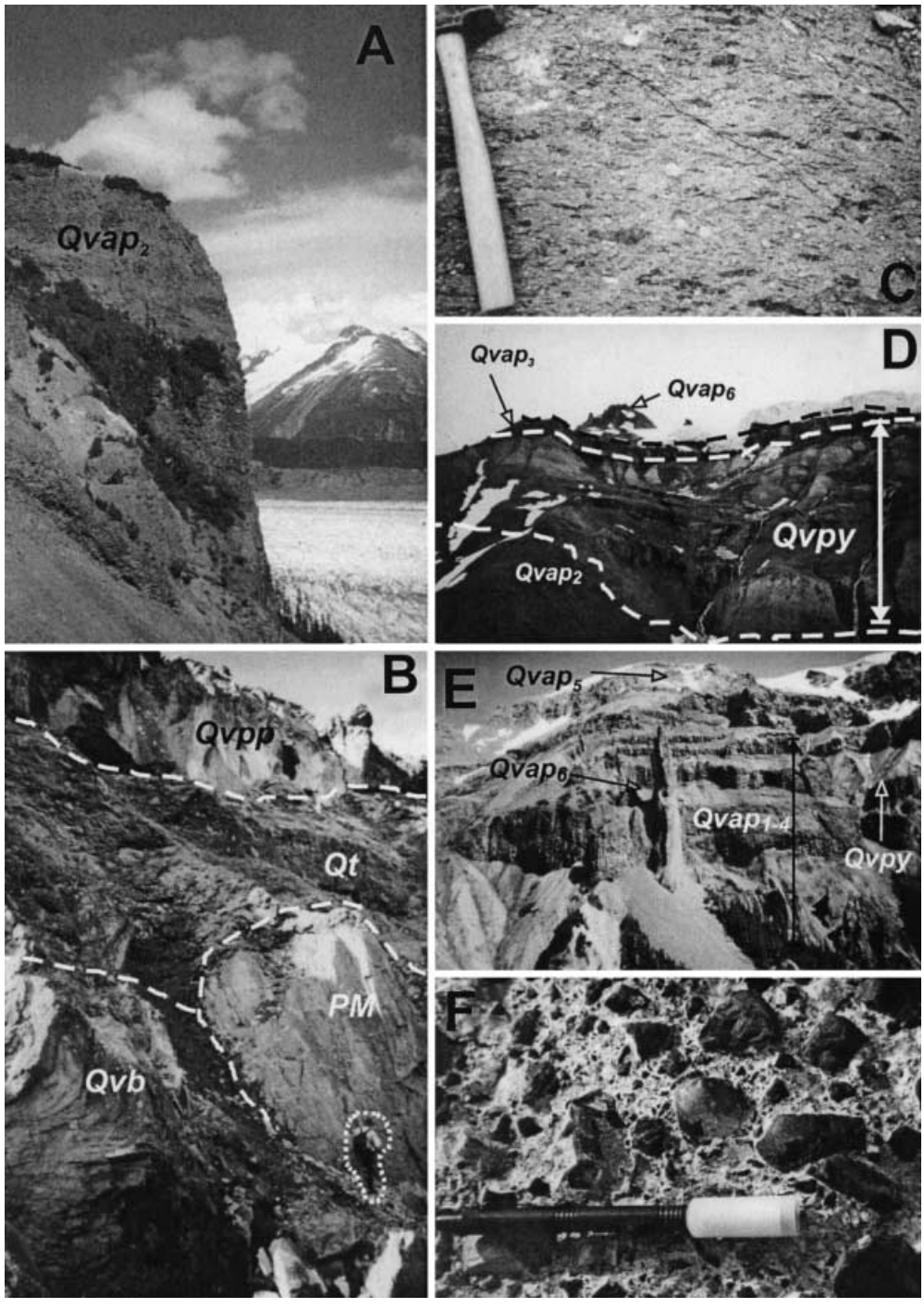

Fig. 4 Morphological and textural features of HMV stratigraphic units. **A** Vertical cliff faces (100–200 m in height) of unit $Qvap_2$ at the Hook (see Fig. 2) on the NE flank of HMV (Fig. 3A, C). The cliffs feature fine-scale, columnar joints and are interpreted as primary quench surfaces of aphyric lava flows that were dammed by valley glaciers. **B** Basement rocks (PM) overlain sequentially by basaltic rocks (*Qvb*) from Little Bear Mountain, glacial till (*Qt*) and post-glacial HMV lava flows (*Qvpp*). The contact between Qvb and PM is vertical. Person (*lower right*) is 1.5 m. **C** Eutaxitic texture in unit Qvpy. Hammer is approximately 30 cm long. **D** Stratigraphic relationships between pyroclastic rocks (Qvpy) exposed on north flank of HMV (see Fig. 3A) and underlying ($Qvap_2$) and overlying ($Qvap_{3,6}$) lava flows (Pointer Ridge deposits; see Fig. 2). Vertical height of section is about 700 m. **E** Volcanic stratigraphy exposed in Slide Canyon (Fig. 2) on the SW flank of HMV. Pinnacle (~100 m high) is a dike of $Qvap_6$ cutting older units, including units $Qvap_{1–5}$. Recessive layers of Qvpy occur between $Qvap_2$ and $Qvap_4$. **F** Angular clasts in monomict breccia associated with massive lava flows of unit $Qvap_5$. Flare pen is 15 cm long

$Qvap_{1,5}$, and (4) the intimate association of hyaloclastite with $Qvap_6$. For example, the morphology of lava flows of $Qvap_{1,2,5}$ are indicative of interactions with ice. Many of the lava flows thicken substantially downslope from a few tens of meters to a few hundred meters (Fig. 4A). The orientation of the jointing seen in many of the cliff faces is consistent with highly irregular to vertical cooling surfaces as well as rapid rates of cooling (e.g., Lescinsky and Fink 2000; Tuffen et al. 2001). The lava flow morphologies and joint orientations are best explained by cooling against steep ice walls (Kerr 1948; Souther 1991a).

Outcrops of lava flows in units $Qvap_{1,5,6}$ always show pervasive jointing that features irregular, small diameter (<1 m) columns (Fig. 5A, B). Several workers (Long and Wood 1986; Bergh and Sigvaldason 1991; DeGraff and Aydin 1993) have suggested that such jointing is characteristic of lava flows cooled in water-rich environments. Bergh and Sigvaldson (1991) interpreted highly jointed lava lobes that are enclosed by monomict breccias, very

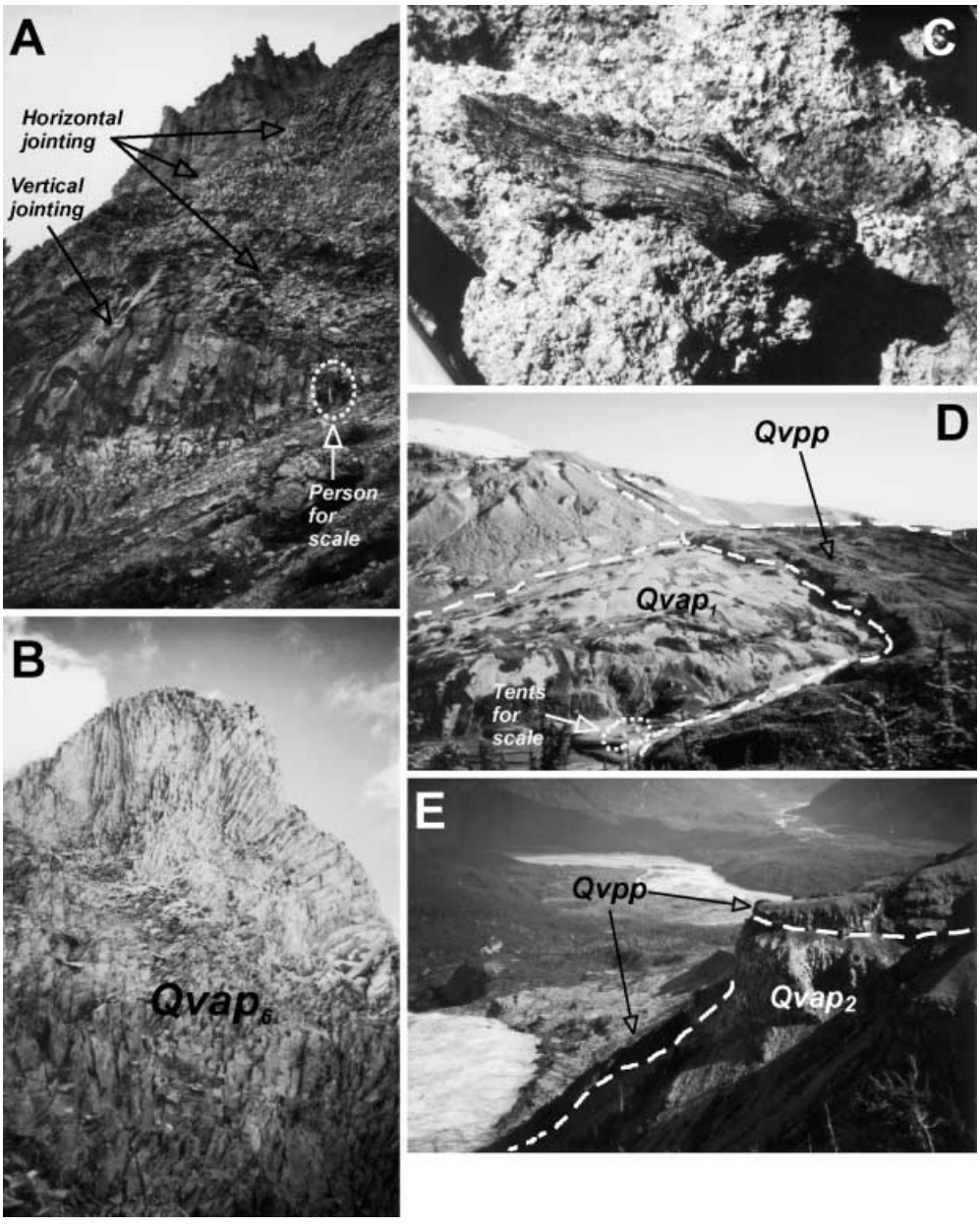

Fig. 5 **A** Pervasive, polygonal jointing in $Qvap_5$ with orientations varying from vertical to horizontal, south-central side of Hoodoo Mountain. Person in *right center* for scale is approximately 1.5 m. **B** Radially-oriented cooling joints (typical spacing ~0.4 m) in unit $Qvap_6$ on north-central side of HMV (at H in Fig. 3). **C** Pumiceous, 10 cm long, ribbon-shaped clast in pyroclastic deposit (*Qvh*) associated with $Qvap_6$ (NW flank of HMV). Matrix appears to be yellow, hydrothermally altered ash. **D** Physiographic expression of the youngest lava flows (Qvpp) exemplified by a lava flow erupted from the northwest flanks of the volcano. Lava vented from areas that are now beneath the icecap and flowed ~3 km down flanks, partly covering cliffs of $Qvap_1$. **E** Remnants of Qvpp lava flows shown draping ~50-m-high cliffs of $Qvap_2$ on the eastern flank of HMV and extending into the valley now occupied by Twin Glacier (*lower left*)

similar in appearance to unit $Qvap_5$, as having formed in subaqueous environments.

The intercalated lava–hyaloclastite association that characterizes unit $Qvap_6$ is interpreted as resulting from eruptions beneath glacial ice. This interpretation is based on the close spatial association between massive, highly jointed lava of $Qvap_6$ and commonly associated carapaces of yellow, glass-rich, pyroclastic breccia. The close spatial association and complex, intermingled contact relationships between the lava and breccia suggest that these deposits are cogenetic. Lava–breccia associations, patterns of lava and clast vesicularity, and columnar jointing are similar to rhyolite lava lobe–breccia associations in Iceland, thought to have been generated in an effusive subglacial eruption (Furnes et al. 1980; Tuffen et al. 2001).

Direct evidence of glacier–volcano interactions at HMV includes glacial striations on lava flows and the intercalation of glacial till and eruptive units found in at least three different stratigraphic intervals, including: (1) at the base of $Qvap_1$ on the southwestern side of HMV, (2) overlying $Qvap_1$(?) on the western side of HMV, (3) bounding vitrophyric pyroclastic deposits on the northwestern flank of HMV, and (4) between unit Qvpp and older basaltic rocks from Little Bear Mountain. Outcrops of $Qvap_2$ on the NW flank of HMV record N–S oriented glacial striations that are consistent with present-day movements of Hoodoo and Twin glaciers (Fig. 3B), however, the elevation of the striations is approximately 500 m above the current level of either of these valley glaciers. Unit Qvpp also has many glacially striated surfaces, but the orientations of these stri-

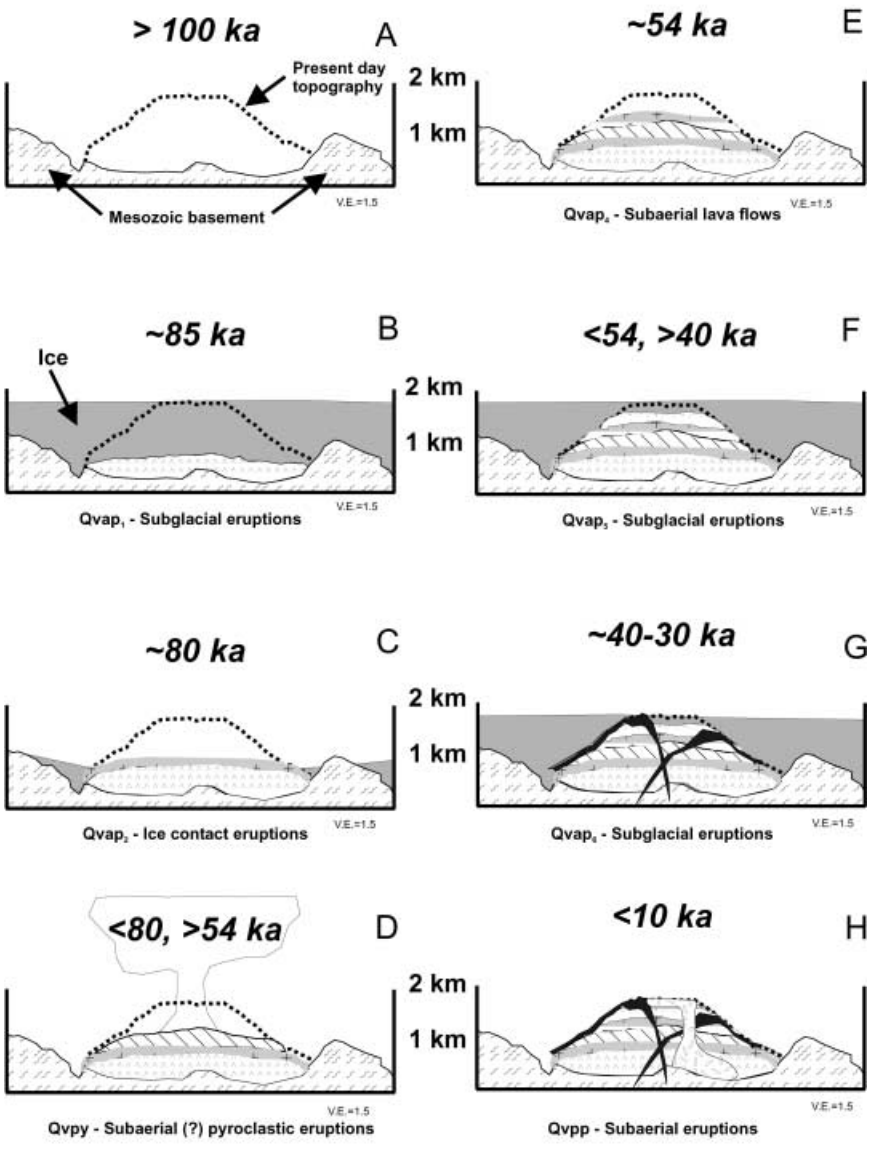

Fig. 6 Physical evolution of HMV depicting: **A** shape of pre-eruptive surface (about 100 ka); **B** subglacial eruption at about 85 ka producing highly jointed lava flows and hyaloclastite; **C** subaerial eruptions at about 80 ka and lava flows dammed against valley glaciers; **D** explosive, pyroclast-producing eruptions between about 80 and 54 ka producing 100 m + thicknesses of welded to non-welded pyroclastic rocks; **E** subaerial eruption of lava flows about 54 ka; **F** major subglacial eruptions between about 54 and 40 ka producing aphanitic lavas and thick carapaces of hyaloclastite; **G** fissure-fed subglacial eruptions between about 40 and 34 ka beneath relatively thin (?) ice; **H** Holocene (<10 ka) subaerial eruptions of highly porphyritic lava from vents buried by present-day icecap

ations suggest that they result from local movements of the summit icecap.

Physical model

On the basis of our stratigraphic, volcanologic, and previously published geochronometric observations, we propose the following model for the physical evolution of HMV (Fig. 6). Prior to the onset of volcanism at HMV, Little Bear Mountain formed by subglacial eruption of alkali olivine basalt at about 240 ka. Its present-day morphology and the presence of glacially striated deposits indicate that Little Bear Mountain was subsequently overridden by glaciers at least once, and most likely several times (Edwards 1997).

The earliest lavas from HMV erupted about 85 ka ($Qvap_1$) and appear to have formed during subglacial eruptions (Fig. 6B). Glacial till that underlies unit $Qvap_1$ near its southwestern flank is strong evidence that HMV originated in an area that had experienced past glaciations. It is not clear whether or not the eruptions that formed $Qvap_1$ completely melted the overlying ice above the juvenile edifice, but, apparently, by about 80 ka, ice was confined to the margins of HMV where lavas of unit $Qvap_2$ ponded and formed the lower cliffs (Fig. 6C). Between the ice-confined lava flows at about 80 ka and the subaerial lava flows of unit $Qvap_4$ at about 54 ka, HMV experienced explosive eruptions forming a thick, pyroclastic sequence (unit Qvpy; Fig. 6D). The environment of eruption for this sequence, while tentatively interpreted as subaerial, is currently being studied in more detail. Subsequent lava flows of $Qvap_4$ preserve no evidence for glacial confinement or interaction; thus, at 54 ka at least the upper flanks of the volcano were apparently free of ice (Fig. 6E).

Formation of succeeding units $Qvap_5$ and $Qvap_6$ occurred during two distinct periods of subglacial eruptions

(Fig. 6F, G). During the formation of $Qvap_5$, overriding glacier ice was thick, perhaps exceeding 2 km (Peltier 1994; Stumpf et al. 2000), and may have covered the entire edifice. Lava flows developed carapaces of ice-chilled breccia and hyaloclastite as they were erupted under the ice. In the waning stages of this episode, between 40 and 30 ka, effusion of lava from isolated vents was replaced by fissure-fed eruptions (unit $Qvap_6$) beneath a relatively thin ice cover aided perhaps by extension related to the substantial thinning of the overriding ice. Thus, the later history (40–30 ka) of HMV was dominated by subglacial volcanism. At about 9 ka, flows of Qvpp erupted subaerially as evidenced by the well preserved and non-glaciated lava levees and blocky lava flow surfaces.

The relatively flat-topped morphology of HMV led Souther (1991a) to refer to Hoodoo Mountain as a "tuya". The flat morphology of a tuya summit is generally ascribed to a capping sequence of subaerial lava deposited on top of a stratigraphic succession dominated by subglacial to subaqueous volcanic fragmental rocks (Mathews 1947; Allen et al. 1982; Hickson 2000). Although the top of HMV does not appear to be capped by subaerial lava, the overall morphology of the edifice has been strongly influenced by interaction between ice and lava, which justifies Souther's original use of the term "tuya".

Chemical evolution of HMV

Mineralogy

The basic mineralogical features of the major map units at HMV, summarized in Table 2, indicate a marked homogeneity in contrast to the diversity of deposit types described above. Mineralogically, all rocks from HMV are nepheline-bearing alkali-feldspar trachyte (IUGS classification, LeMaitre 1989) and contain euhedral to

Table 2 Mineralogy[a] of major HMV map units (after Edwards et al. 2000). The minerals were identified by light microscope and SEM with EDS capability

Unit	Phenocryst[a,b] (%)	Groundmass[c]	Textural notes
$Qvap_{1–5}$	AF (5–10) Cpx (1–5) Mt (1–5)	AF, Cpx, Mt, Ne, Ccn	Aphanitic Holocrystalline Trachytic
$Qvap_6$	AF (1–5) Cpx (1–5) Mt (1–5)	AF, Cpx, Mt	Holo-hyalocrystalline Aphanitic Trachytic
Qvpp	AF (15–20) Cpx (1–5) Mt (1–5)	AF, Cpx, Mt, Ne	Trachytic Holocrystalline Glomerocrystic Rare gabbroic inclusions

[a] Includes phenocrysts (>0.5 mm) and microphenocrysts (<0.05 mm
[b] All rocks contain phenocryst assemblage of AF, Cpx, Mt
[c] *AF* Alkali-feldspar; *Cpx* augite; *Mt* magnetite; *Ne* nepheline; *Ccn* cancrinite

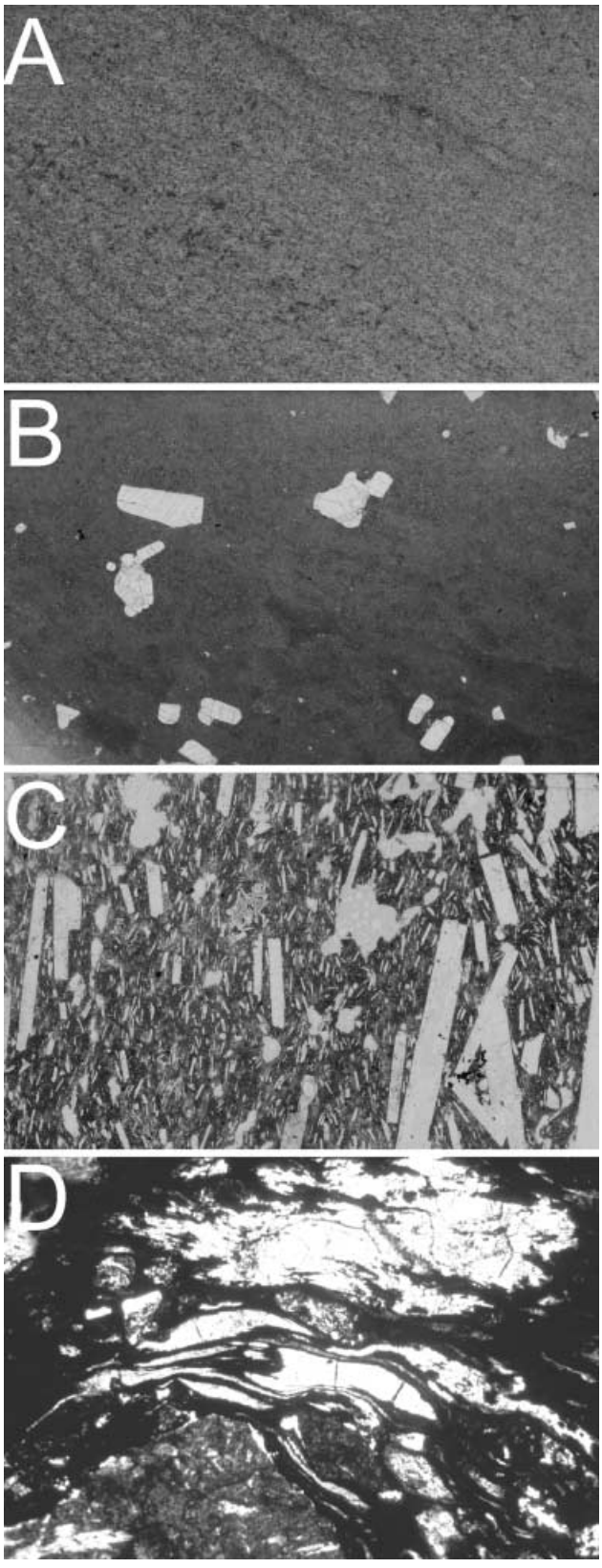

Fig. 7 Plane-polarized scanned images of HMV thin sections, showing **A** aphanitic character of $Qvap_2$; **B** weakly alkali-feldspar porphyritic $Qvap_5$; **C** highly porphyritic alkali feldspar–clinopyroxene–magnetite Qvpp with trachytic texture; **D** eutaxitic texture in Qvpy. Fields of view for **A**–**C** are 2.5×3.5 cm and **D** is 1×2 cm

Table 3 Representative major (wt%) and rare earth element (ppm). Compositions of volcanic units from Hoodoo Mountain volcano. b.d. Below detection

Sample	93-29	93-74	94-76	94-62	94-165	94-108	94-2	94-98
Unit	Qvap	Qvap2	Qvap	Qvap6	Qvh	Qvpp	Qvb	Qvap
TAS[a]	Ph	Ph	Tr	Ph	Ph	Ph	Ba	Ph
SiO_2	58.4	59.2	64.1	56.9	59.9	59.0	45.5	58.1
TiO_2	0.25	0.31	0.30	0.23	0.37	0.28	3.35	0.31
Al_2O_3	15.3	16.3	15.4	15.7	14.5	16.5	16.0	15.2
Fe_2O_3	4.5	2.8	3.2	5.3	2.8	4.5	4.2	1.8
FeO	4.1	4.8	2.7	3.5	6.4	3.2	8.7	6.7
MnO	0.21	0.2	0.15	0.21	0.24	0.19	0.19	0.21
MgO	b.d	b.d.	0.06	b.d.	0.10	0.21	5.53	b.d.
CaO	1.06	1.68	0.63	1.04	1.53	1.65	10.2	1.39
Na_2O	8.3	7.6	6.1	8.8	8.9	7.6	3.1	9.2
K_2O	4.61	5.15	5.13	4.77	4.59	4.94	1.35	4.66
P_2O_5	0.04	0.06	0.05	0.02	0.08	0.06	0.96	0.06
H_2O (T)	2.5	1.2	0.7	3.3	0.4	1.2	1.3	2.0
CO_2 (T)	0.2	0.3	1.6	b.d.	b.d.	b.d.	b.d.	0.1
S(T)	0.03	0.03	0.02	0.03	0.05	b.d.	0.05	0.04
Total	99.5	99.63	100.14	99.8	99.86	99.33	100.43	99.77
Fe_2O_3 (T)	9.1	8.1	6.2	9.2	9.9	8.1	13.87	9.2
La	130	95	100	130	150	120	31	110
Ce	260	190	210	260	290	230	70	230
Pr	33	23	26	32	36	28	9.3	27
Nd	130	88	100	120	140	110	41	110
Sm	27	17	21	25	28	22	8.8	22
Eu	3.5	2.0	2.5	3.6	3	2.5	3.4	3.1
Gd	26	16	22	26	27	22	9.0	21
Tb	4.1	2.7	3.4	4.1	4.3	3.5	1.2	3.4
Dy	24	16	19	23	24	20	6.2	19
Ho	4.8	3.1	3.6	4.5	4.8	3.8	1.1	3.7
Er	13	8.7	9.4	12	13	10	2.6	9.8
Tm	1.9	1.3	1.6	1.9	2.1	1.7	0.40	1.6
Yb	11	7.9	9.4	11	12	9.7	2.2	9.2
Lu	1.5	1.2	1.5	1.6	1.6	1.5	0.3	1.3

[a] *Ph* Phonolite; *Tr* trachyte; *Ba* basalt

subhedral alkali feldspar (AF; dominantly anorthoclase), magnetite (Mt) and Fe-rich augite (Cpx) as phenocrysts and in the groundmass. Nepheline (Ne) and a Na–Al–Si–Cl-bearing phase (possibly cancrinite) are also found in the groundmass of some samples. Massive lava flows (e.g., Qvap and Qvpp) vary from aphyric (<1% phenocrysts) to abundantly porphyritic (>15% phenocrysts) (Fig. 7A–C), but all samples have an aphanitic matrix. Most lavas are holocrystalline to cryptocrystalline and trachytic to pilotaxitic. Volcanic glass is only abundant in pyroclastic deposits (e.g., unit Qvpy; Fig. 7D). Higher stratigraphic units (e.g., unit Qvpp) have higher abundances (15–20 vol%) and larger sizes (>2 cm) of AF phenocrysts. The youngest Qvpp lavas commonly contain glomerocrysts of AF, Mt, and Cpx, and locally inclusions of troctolite and gabbro.

Major element geochemistry

Major and rare earth element (REE) abundances for a group of representative HMV samples are reported in Table 3; a complete suite of chemical compositions is found in the electronic supplementary material. The analyses were completed at the Geological Survey of Canada; see Russell and Hauksdóttir (2000) for details pertaining to the methods of sample preparation, analysis, and estimates of analytical precision.

The compositional range of the HMV phonolites and trachytes (Fig. 8A) is small relative to the two other large volcanic centers of the Stikine subprovince: Mount Edziza and Level Mountain; all HMV samples but one contain between 56 and 60 wt% SiO_2 (Fig. 8A). Samples of volcanic glass from unit Qvpy and the majority of samples of $Qvap_{1–5}$ are phonolite or transitional between trachyte and phonolite. Samples of unit Qvpp plot as trachyte, near the phonolite boundary.

Samples of HMV lavas (n=48) are nepheline normative except for a single quartz normative sample from the base of the volcano (94BRE76). Within the Ne–Qtz–Ks ternary projection, HMV rocks plot along the Ab–Or join or below the join in the undersaturated field (Fig. 8B), as expected from the presence of modal Ne and the Ne-normative character of these rocks. Samples of HMV lavas also have normative acmite and are chemically peralkaline (Fig. 8C). However, samples of glass from pyroclastic units are the most sodic and agpaitic (Fig. 8C), whereas samples of porphyritic Qvpp are slightly less agpaitic compared to samples of Qvap with similar values of K/Na. The Qvpp samples are also the

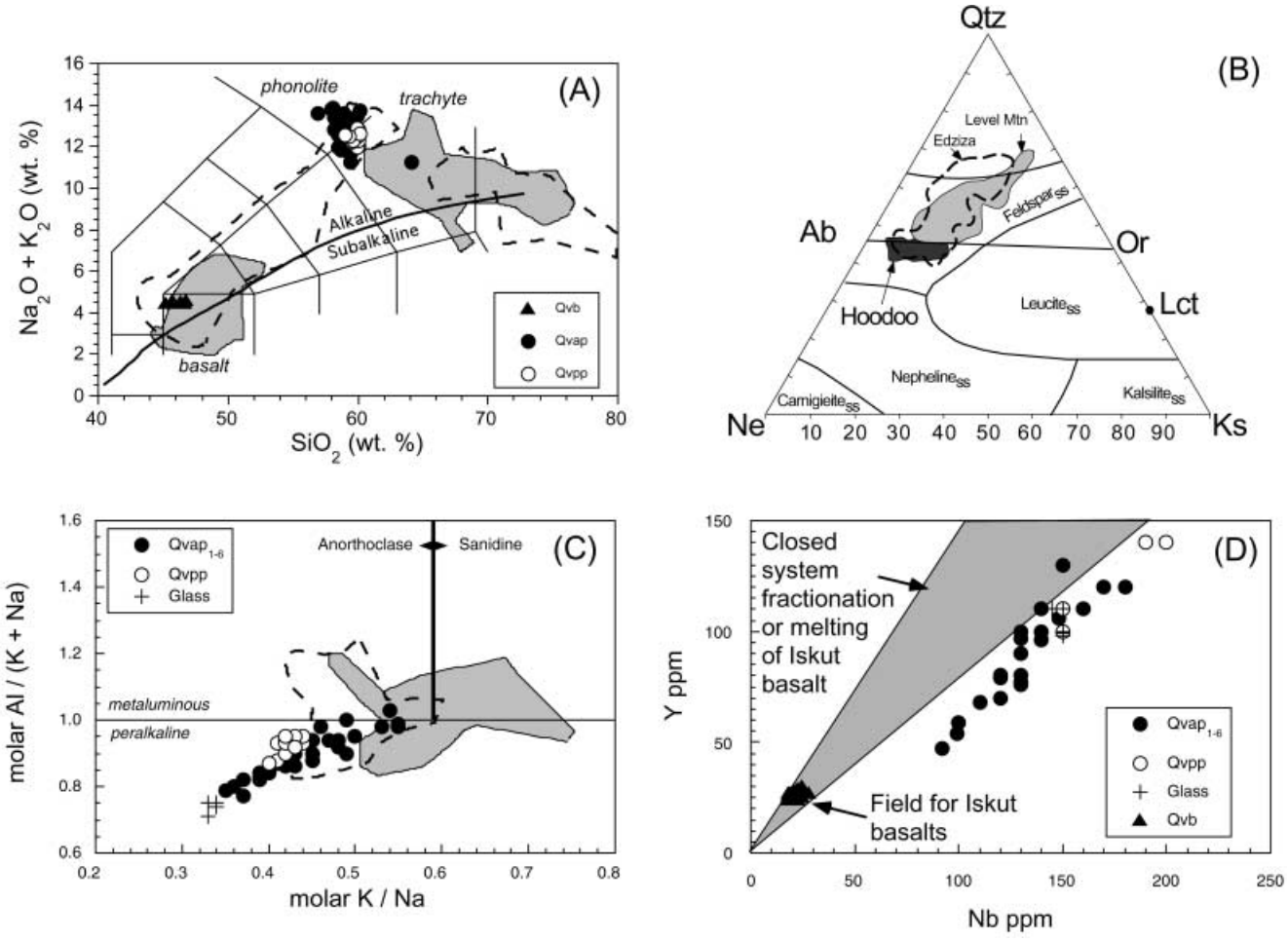

Fig. 8 Chemical compositions of volcanic rocks from HMV compared with rocks from Edziza (*shaded fields* in **A**, **B**, **C**; see Fig. 1B) and Level Mountain (*dashed fields* in **A**, **B**, **C**; see Fig. 1B). **A** TAS classification for volcanic rocks (Le Bas et al. 1986; LeMaitre 1989). Alkaline and subalkaline fields in **A** are from Irvine and Baragar (1971). **B** Nepheline–Quartz–Kalsilite ternary projection (Fudali 1963). **C** Molar Al/(K+Na) versus molar K/Na. **D** Nb ppm versus Y ppm

most enriched in many incompatible trace elements (e.g., Y and Nb, Fig. 8D).

The homogeneous and undersaturated nature of HMV lavas distinguishes them from the intermediate to felsic volcanic rocks found at Level Mountain and Mount Edziza (Fig. 8A–C). Samples from units at Level Mountain and Edziza include quartz-saturated peralkaline rhyolites in addition to quartz-free peralkaline and metaluminous trachytes (Hamilton 1981; Souther and Hickson 1984; Souther 1992). HMV samples are the most silica-undersaturated rock types in the Stikine subprovince (Fig. 8B). Compared with trachytes from Level Mountain and Edziza, the HMV trachytes and phonolites are more agpaitic (lower values of Al/(Na+K)) and also more sodic (lower values of K/Na) (Fig. 8C). More than 90% of the samples from Level Mountain, Edziza, and HMV have K/Na ratios less than that for sanidine (0.59); this is consistent with the dominance of phenocrystic anorthoclase in HMV rocks. Virtually all HMV lavas are peralkaline whereas at Mount Edziza and at Level Mountain lavas are peralkaline and metaluminous in subequal proportions.

Rare earth element geochemistry

Rare earth element (REE) compositions of HMV rocks are enriched relative to values for primitive mantle (Fig. 9A) and values for average basalt from the Iskut volcanic field (Fig. 9B). Most HMV rocks show relatively constant abundance patterns and levels of enrichment. Relative to primitive mantle, HMV samples show 100–200 times enrichment in LREE, 1–20 times enrichment in HREE, and greater fractionation of LREE (La/Sm_n >3) than HREE (Gd/Lu_n <2.2). All samples of phonolite and trachyte show a pronounced negative Eu anomaly. The variations in normalized REE patterns among individual map units (e.g., $Qvap_{1–6}$ vs. Qvpp) are small and only slightly larger than the variations found within individual units (Figs. 9A, B).

Differences between HMV map units are emphasized by normalizing the REE data for HMV samples to the composition of a sample of aphyric HMV glass

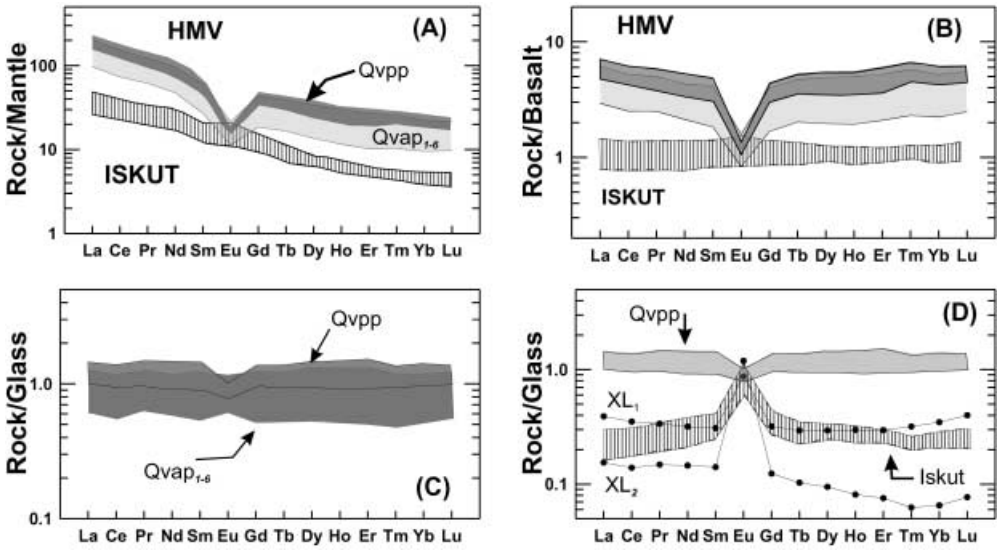

Fig. 9A–D Rare earth element compositions of volcanic rocks from HMV. **A** Compositions of HMV rocks are normalized to primitive mantle (McDonough and Sun 1995) and compared with basalts from the Iskut volcanic field (*striped pattern*), including basaltic rocks from Little Bear Mountain. HMV compositions are shown as two groups, including units $Qvap_{1–6}$ and samples of Qvpp and glassy blocks from hyaloclastite units. **B** The same data as in **A** normalized to the most magnesian basalt from Lava Fork field (Fig. 1; Russell and Hauksdóttir 2000). **C** REE compositions of $Qvap_{1–6}$ and Qvpp are normalized to volcanic glass (94BRE98; Table 3). **D** Qvpp lavas normalized to volcanic glass (94BRE98; Table 3) and compared with basaltic rocks from the Iskut volcanic field (*shaded*) and to xenoliths in basaltic rocks from Little Bear Mountain (XL_1 and XL_2)

(94BRE98 from unit $Qvap_6$, Table 3; Fig. 9C, D). In general, the REE patterns thus normalized are flat, indicating little REE fractionation between individual flow units (Fig. 9C, D). Europium is the exception. Most samples from $Qvap_{1–6}$ show little to no Eu anomaly relative to the reference glass, whereas, almost all Qvpp lavas show negative Eu anomalies (Fig. 9C). Other differences in REE enrichment include slightly less enrichment in samples from units $Qvap_{1–6}$ and slightly more enrichment in samples from Qvpp (Fig. 9C). Basalts from the Iskut volcanic field show substantially less overall REE enrichment, have a slight positive slope for LREE, and a large, positive Eu anomaly (Fig. 9D).

Chemical evolution

The chemical evolution of HMV encompasses production of >17 km^3 of compositionally restricted phonolite and trachyte over a 80,000-year time interval, contemporaneously with basaltic volcanism represented by the nearby Iskut volcanic field (Fig. 1C). Although the compositional characteristics of the Iskut basalts can be explained by derivation from asthenospheric sources (e.g., Francis and Ludden 1990; Carignan et al. 1994; Cousens and Bevier 1995; Edwards and Russell 2000) and minor crustal contamination (Russell and Hauksdóttir 2000), the large volume of phonolite and trachyte at Hoodoo Mountain requires an alternative explanation.

Trachyte and phonolite melts can result from diverse processes, including (1) partial fusion of alkali olivine basalt (Hay and Wendlandt 1995; Kaszuba and Wendlandt 2000), (2) fractional crystallization of basanitic or alkali olivine basaltic melts (e.g., Le Roex et al. 1990; Kyle et al. 1992; Kuntzmann and Blasse 2000), and (3) coupled fractional crystallization and assimilation (e.g., Kyle et al. 1992; Wilson et al. 1995; Edwards and Russell 1998) In the case of the HMV, partial fusion of alkali olivine basalt is unlikely for at least three reasons. Firstly, the peralkaline nature of HMV lavas is not consistent with melting of a plagioclase-rich source. All phonolite and trachyte glass compositions reported by Kaszuba and Wendlandt (2000) are metaluminous. Secondly, ratios of incompatible elements for samples of HMV lavas and for basaltic samples from the Iskut volcanic field are not co-linear (Fig. 8D). This is inconsistent with the HMV lavas being directly derived from Iskut basalt via closed system melting. Finally, if the HMV lavas were derived solely by closed system partial melting of basaltic crust similar in REE composition to Iskut basalt samples, it would be expected that the HMV samples would also have positive Eu anomalies, not large negative ones (Fig. 9). Trace element data also rule out derivation of HMV lavas from closed system fractional crystallization of basanite and/or alkali olivine basalt (Fig. 8D).

We propose that HMV phonolites and trachytes derive from AFC involving primary mantle-derived alkali olivine basaltic magmas and granitic crustal rocks. This scenario is supported by a number of lines of evidence. At HMV, the ratio of basalt (Little Bear Mountain) to phonolite is extremely low, 0.3 to >17 km^3, particularly compared with the other two major centers in the Stikine subprovince, Mount Edziza (1:1; Souther 1992) and Level Mountain (4:1; Hamilton 1981). We argue that the apparent lack of large volumes of basalt within the Iskut

region is most consistent with an origin by coupled fractional crystallization and assimilation. The alkali olivine basalt at Little Bear Mountain and the rest of the Iskut volcanic field (Fig. 1C) is clear evidence of widespread, contemporaneous mantle-derived, mafic magmatism. These basaltic magmas carry abundant xenoliths and xenocrysts of crustal material (Stasiuk and Russell 1989; Edwards and Russell 2000; Russell and Hauksdóttir 2000), many of which show evidence of melting during transport and that have been identified as contaminants in many of the basaltic magmas in the Iskut volcanic field (Cousens and Bevier 1995; Edwards 1997; Russell and Hauksdóttir 2000). Similar direct evidence of magmatic assimilation is common at other volcanic centers throughout the NCVP including Level Mountain (Hamilton 1981), Mount Edziza (Souther 1992), the Tuya Buttes area (Watson and Mathews 1948), Alligator Lake (Eiche et al. 1987), Fort Selkirk (Francis and Ludden 1990), and Prindle volcano (Foster et al. 1966).

To test the efficacy of the AFC process, we have computed model liquid lines of descent for six different AFC scenarios (Table 4, Fig. 10A) using the thermodynamics-based program MELTS (Ghiorso and Sack 1995). The model paths are calculated using a parental magma of alkali olivine basaltic composition, consistent with basalt from the Iskut volcanic field (Lava Fork, SH-44), and include closed system fractional crystallization (F), and fractional crystallization coupled to assimilation of granite (G), quartz (Q), albite (An10), K-feldspar (Kfs) and Mg-rich biotite (B) (after Edwards and Russell 1996).

Fractional crystallization of alkali olivine basalt is sufficient to produce liquids approximately equivalent to HMV rocks, but the system is over 80% crystallized by the time it produces trachyte. However, AFC processes involving the incorporation of granitic material allow the system to reach the field of HMV samples while a substantial melt fraction remains (Fig. 10A); thus, compared with AFC processes, closed system fractional crystallization is a much less efficient means to produce magmas similar to the HMV samples. Scenarios involving assimilation of individual constituent minerals of the granite are used (Fig. 10A) to show the relative effects of increasing the modal amounts of these phases in the average crustal contaminant. Increasing quartz content, for example, drives the system away from the compositional field for HMV rocks. Conversely, increasing the K-feldspar or Mg-biotite content of the average crustal material facilitates reaching the HMV field; assimilation of K-feldspar-rich granitoids produces compositions equivalent to HMV phonolites at a point where 50% of the original mass is still melt. These simulations clearly demonstrate that the volumes of derived phonolitic magma available are maximized by AFC processes, relative to the volumes derived from fractional crystallization alone.

These model differentiation paths are also unique in their physical properties: melt density and percent melt remaining in the system (F) (Fig. 10B). Lower density values enhance buoyancy-driven extraction of magma

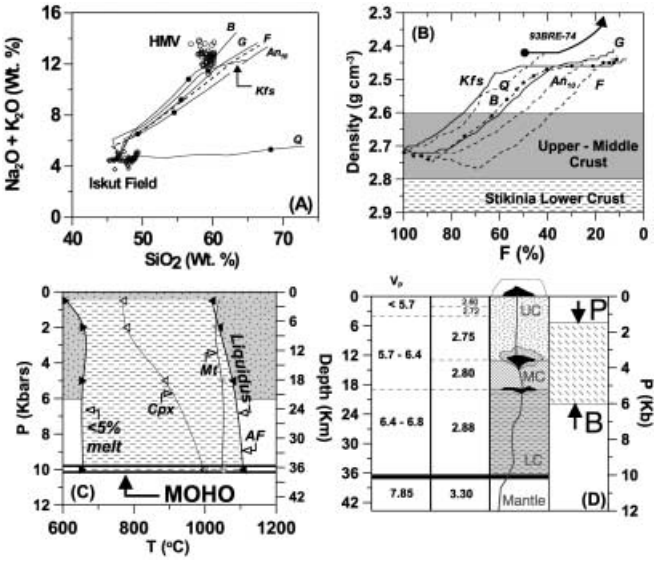

Fig. 10A–D Chemical model for origins of phonolitic magmatism at HMV. **A** Compositions of HMV rocks and Iskut basalts shown as $Na_2O + K_2O$ vs. SiO_2 and compared with liquid lines of descent produced by AFC processes involving alkali olivine basalt and crustal components (Table 4; see text), including: quartz (*Q*), K-feldspar (*Kfs*), plagioclase (*An10*), Mg-rich biotite (*B*), and granite (*G*). Closed system fractionation path (*F*) is also shown. *Filled circles* on paths indicate where the percent melt is 50% of the original mass. **B** The same model paths plotted as melt density vs. percent melt (F%) in system. Density of Stikinia crustal rocks (*shading*) are from (Hammer et al. 2000). *Heavy line* shows low pressure fractionation path for HMV phonolite (Table 4). **C** Equilibrium P–T crystallization phase diagram calculated for HMV phonolite. See Table 5 for details of MELTS output used to construct diagram. *Dashed pattern* shows the P–T region of stability for the phase assemblage (*AF* alkali feldspar; *Mt* magnetite; *Cpx* hedenbergite) expected for HMV magmas. *Lines with symbols* represent near-solidus (<5% melt) conditions (*line on the left with solid triangles*) and temperatures of first appearance for Cpx (*line with open triangles*), Mt (*line with shaded triangles*), and AF (*line on right with solid triangles*). Phenocryst assemblages in Iskut basalts (stippled pattern) suggest crystallization at pressures below 6 Kb. **D** The crustal properties of Stikinia as constrained by seismic data including Vp and density, used to define thicknesses of upper (*UC*), mid- (*MC*) and lower (*LC*) crust and depth to MOHO (Hammer and Clowes 2000; Hammer et al. 2000). Panel also portrays ascent of asthenospheric-sourced basaltic magmas (*black*) to mid to upper crustal depths where AFC processes produce peralkaline phonolitic magmas of HMV. The depth of AFC processes (*right-hand panel*) is constrained by phenocrysts in basaltic rocks of the Iskut field (B, maximum) and based on the interpretation that AF, instead of Mt, is the liquidus phase in HMV lavas (P, minimum; see **C**)

from the crustal lithosphere. Reaching phonolite compositions at higher values of F produces a greater volume of phonolite for a given mass of parental basalt. Again, closed system fractionation is a less viable explanation for HMV because, not only are values of F low when the phonolite field is reached, but the density of the residual melts are equivalent or higher than the densities of the crustal rocks underlying HMV (e.g., Hammer and Clowes 2000). The melts produced by this path are unlikely to erupt under lithostatic pressures until the system achieves 60% crystallization. Conversely, melts resulting

Table 4 Select model parameters from calculated AFC paths derived from fractional crystallization (*F*) of alkali olivine basalt (SH-44 from Lava Fork; Russell and Hauksdóttir 2000) and assimilation of granite (*G*), quartz (*Q*), plagioclase (An_{10}), alkali feldspar (*Kfs*), or Mg-rich biotite (*B*) (for details see Edwards and Russell 1996). All calculations were performed by MELTS (Ghiorso and Sack 1995). Assimilation scenarios consumed 20 g of material for 100 g of initial melt at a rate of 1 g per 5 °C cooling (e.g., Edwards and Russell 1996)

Path	Crystallization sequence (Saturation T °C)	Feldspar composition	Properties at F=50[a]	
			Solid mass/100 g	ρ_M (g cm^{-3})
F	Pl (1175); Ol (1170); Spl (1125); Cpx (1120)	$An_{71\text{-}3}$	47	2.70
G	Pl (1170); Ol (1170); Spl (1125); Cpx (1115); AF (1045)	$An_{70\text{-}26}$ $Or_{43}An_9Ab_{48}$–$Or_{49}An_3Ab_{47}$	60	2.55
Q	Pl (1170); Ol (1170); Opx (1115); Spl (1110); Pig (1060); Rhm (990)	$An_{68\text{-}34}$	70	2.47
An_{10}	Pl (1175); Ol (1170); Spl (1130); Cpx (1110)	$An_{71\text{-}5}$	64	2.60
Kfs	Pl (1170); Ol (1170); Spl (1125); Cpx (1115); AF (1060)	$An_{71\text{-}35}$ $Or_{52}An_8Ab_{39}$–$Or_{61}An_2Ab_{37}$	69	2.46
B	Pl (1170); Ol (1160); Spl (1120); Cpx (1115); AF (1050)	$An_{71\text{-}32}$ $Or_{50}An_8Ab_{42}$–$Or_{50}An_4Ab_{46}$	71	2.51

[a] Parameters are reported for the point on the path at which there remains 50% melt

Table 5 Equilibrium crystallization path for HMV phonolite shown in Fig. 10. Model calculations are based on MELTS program (Ghiorso and Sack 1995) and use aphyric lava ($Qvap_2$; 93-74; Table 2) as melt composition. Original melt is assumed to contain 1 wt% H_2O and oxygen fugacity is fixed at FMQ

P (GPa)	Phase (Saturation T °C)	Feldspar composition	Pyroxene composition
500 MPa	Mt (1038); AF (1018); Pl (989); Cpx (769)	$Or_{41}Ab_{51}$–$Or_{67}Ab_{33}$ $Ab_{62}An_{17}$–$Ab_{84}An_8$	$Hd_{63\text{-}66}$
0.2	AF (1038); Mt (1048); Cpx (779)	$Or_{49}Ab_{46}$–$Or_{63}Ab_{36}$ Ab65An_{13}–Ab_{83}An7	$Hd_{62\text{-}66}$
0.5	AF (1077); Mt (1048); Cpx (887)	$Or_{48}Ab_{46}$–$Or_{67}Ab_{32}$ $Ab_{62}An_{13}$–$Ab_{84}An_6$	$Hd_{64\text{-}57}$
1	AF (1105); Mt (1046); Cpx (996); Bt (656)	$Or_{47}Ab_{47}$–$Or_{74}Ab_{26}$ $Ab_{64}An_7$–$Ab_{88}An_2$	$Hd_{62\text{-}36}$
1.5	AF (1101); Grt (1090); At (1031); Cpx (951)	$Or_{40}Ab_{52}$–$Or_{81}Ab_{19}$ $Ab_{68}An_3$–$Ab_{92}An_1$	$Hd_{49\text{-}26}$
500 MPa (dry)	AF (1084); Mt (1074); Cpx (886); Ne (855)	$Or_{39}Ab_{52}$–$Or_{50}Ab_{48}$ $Ab_{64}An_{14}$–$Ab_{79}An_5$	$Hd_{57\text{-}61}$

from AFC processes involving granite or K-rich granitic material become buoyant relative to Stikine crust at 30% crystallization (i.e., melt fractions as high as 70%; Fig. 10B). The densities of melts along these paths compare favorably with the densities of melts computed for HMV phonolites and their fractionation products (Fig. 10B, heavy line). In summary, the AFC processes that involve alkali olivine basaltic magma and incorporation of granitic rocks are clearly capable of producing extractable, voluminous magmas similar in composition to the HMV phonolites.

Several lines of evidence are consistent with the AFC processes taking place at mid- to upper crustal depths. Edwards and Russell (2000) and Trupia and Nicholls (1996) have shown that, for many NCVP basaltic magmas, crystallization of phenocryst assemblages occurred at pressures between 0.4 and 0.8 GPa or at depths between 18 and 29 km. Phenocryst assemblages in lavas from the Iskut volcanic field suggest crystallization at pressures up to 0.6 GPa. Secondly, we have calculated an equilibrium crystallization map for HMV phonolite using MELTS (Table 5, Fig. 10C). These calculations, used in conjunction with the observed petrography, limit the ponding of the magma and crystallization of the phenocryst assemblage (Afsp >>Mt >Cpx) to confining pressures >0.15 GPa. Lastly, recent data from Lithoprobe have produced a geophysical picture of the part of Stikinia that underlies HMV (Hammer et al. 2000; Hammer and Clowes 2000). The seismic data show the depth to the MOHO (~37 km) and the nature of density stratification in the crust. The crust of Stikinia features a substantially denser lower crust (2,850–2,900 kg m^{-3}) between 37 and 19 km depth (Hammer and Clowes 2000). The mid-crust (19–13 km depth) is defined by a

2–3% reduction in density (2,800 kg m^{-3}) and the transition to upper crust (13 km) coincides with an additional 2–7% decrease in average density (2,600–2,750 kg m^{-3}; Fig. 10D). Hyndman and Lewis (1999) suggest that, because of the high ambient heat flow in the Cordillera, the brittle–ductile transition may be situated at a depth of 10–12 km.

On the basis of these observations, the transition between upper and middle crust is probably marked by a substantial change in composition and rheology. We suggest that this pronounced break in properties of crustal rocks serves as a filter to some asthenosphere-derived magmas. Magmas derived from relatively deeper levels of the asthenosphere are compensated for by lithostatic forces that allow them to traverse the entire crustal lithosphere and erupt; many of these magmas are nearly aphyric and entrain mantle-derived xenoliths attesting to their relatively fast and uninterrupted path through the lithosphere (Edwards and Russell 2000). A second class of magma is represented by basalt erupted in the Iskut volcanic field and many other places within the NCVP (Edwards and Russell 2000). These lavas are olivine ± plagioclase porphyritic, never contain mantle-derived xenoliths, but commonly entrain crustal xenoliths and xenocrysts. These magmas have probably ponded within the crustal column and undergone crystallization prior to erupting (Fig. 10C, D). The phonolitic rocks at HMV are an expression of these stalled magmas continuing to interact with the crust and creating new melt compositions.

Glacial–chemical coupling

The physical evolution and eruption style of HMV is largely shaped, if not controlled, by the proximity of large regional sheets of ice that have periodically enclosed the entire edifice (e.g., at about 85 and about 40–20 ka). In the past, Cordilleran ice masses have reached 2–3 km above present sea level; during Fraser glaciation the ice sheets are estimated to have been between 1 and 2 km thick (Peltier 1994; Stumpf et al. 2000; Dixon et al. 2002). Furthermore, HMV phonolitic magmas can be shown to result from the ponding of basaltic magmas at relatively shallow (12–13 km) crustal depths and the subsequent assimilation of K-rich granitic crustal rocks. We now ask the question: can AFC processes and ice loading of the lithosphere operate in tandem to cause eruptions of HMV?

Below, we have explored the potential for coupling between the extent of AFC processes and fluctuations in the thickness of ice sheets to facilitate the eruption of crustally stored magma. In these calculations we assume the following: (1) basaltic magma (ρ_m=2,750 kg m^{-3}) is originally stored in the crust at a depth (X_c) coinciding with the upper to middle crust transition as constrained by seismic data (e.g., 13 km; Hammer et al. 2000); (2) the overlying crust is given a constant density (ρ_c)of 2,700 kg m^{-3}; (3) the density (ρ_m) of the magma is changed by assimilation of granitoid (G in Fig. 10B) and is related to the extent of AFC by the value of F (%):

$$\rho_m = 4F + 2348; \quad (1)$$

and, (4) ice sheets loading the crust have density 900 kg m^{-3} and thickness (T_i). Lastly, we assign a strength of 10 MPa to upper crustal rocks ($\varnothing_c$), which also must be overcome to permit the ascent and eruption of magma. Based on this configuration, the total lithospheric pressure at the depth where basalt magma is stored at the base of the upper crust is:

$$P_L = 9.8\,[900T_i + \rho_c X_c] \quad (2)$$

The pressure at the base of the column of erupted magma is then given by:

$$P_M = 9.8(X_c + h)\rho_m \quad (3)$$

where h is the height to which magma is supplied depending on whether the eruption is subglacial (h=0) or supraglacial (h=T_i). The conditions for eruption, therefore, are met at:

$$P_L - P_M > \varnothing_c \quad (4)$$

Supraglacial eruptions, possibly represented by some $Qvap_6$ deposits at HMV, require that magma is supplied to the upper surface of the ice sheet. This limiting behavior implies the following relationship between the variables T_i (km) and F (%)

$$T_i > [889 - 13F] / [362 + F] \quad (5)$$

and is mapped as a solid line in Fig. 11. The fraction of melt (F) serves as a proxy for the extent of AFC process (e.g., Fig. 10A). AFC processes operate on HMV parent magmas to create more buoyant magma (Fig. 10B), which increases the opportunity for eruption at the upper ice surface. Increasing ice thickness limits the possibilities of supraglacial eruptions. The supraglacial eruption window for HMV, therefore, is defined by the limiting values of ice thickness of 0 and 2 km (the maximum for HMV) and the corresponding values of F (68–12%). The main conclusion of this relationship is that supraglacial eruptions are favored by thinner ice sheets and by greater degrees of AFC.

Subglacial eruption of crustally stored magmas represents another limiting type of behavior, where magma is supplied only to the base of the ice sheet (e.g., h=0). This situation is modeled in terms of T_i (km) and F (%) by the inequality:

$$T_i > 0.058F - 3.95 \quad (6)$$

This relationship is plotted in Fig. 11 as a solid curve (on the left) and defines the critical values of *Ti–F* that exactly support subglacial eruptions at HMV. At lower values of T_i (e.g., thin ice) and F (dense magma) no eruptions occur (region A in Fig. 11). Combinations of T_i–F values that exceed the critical curve will support eruptions at the base and within the ice sheet (region B in Fig. 11). The critical curve for subglacial eruptions shows a markedly different relationship between the role

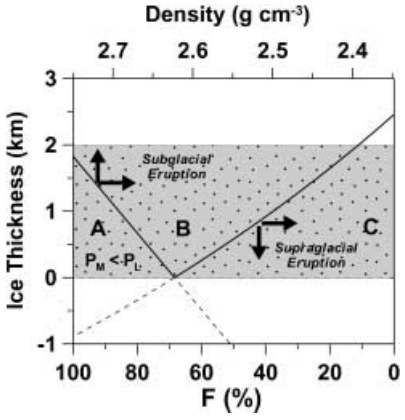

Fig. 11 Minimum conditions for lithostatic-driven eruption of magmas stored at the base of the upper crust (13 km) are plotted as F (% melt fraction) for AFC path shown in Fig. 10A vs. thickness of regional ice sheet. AFC processes operate on basaltic magmas to create buoyancy by changing the melt density (Fig. 10B). The *shaded region* shows the maximum estimates of ice thickness for the region surrounding HMV since 80 ka based on morphology and textures of volcanic deposits. Solution space has three distinct domains. *A* No eruption where ice load is insufficient to compensate for relatively high density of magma. *B* Subglacial to within ice eruptions are supported by ice loading or by decreasing magma density due to AFC processes. *C* Supraglacial eruptions are driven by AFC processes creating buoyant magma or by decreases in ice thickness. The *solid lines* map the minimum conditions required for subglacial (*left curve*) or supraglacial (*right curve*) eruptions. They have opposite slopes. Subglacial eruptions require only that magma is supplied to the base of the ice sheet and, therefore, ice loading of the crust increases the opportunity for eruption of magma that has undergone less chemical modification (F>68%). Loading and thickening of the crust by ice operates against supraglacial eruption and requires substantial modification of magma properties by AFC processes (e.g., F<68%)

of ice loading and assimilation than did the supraglacial eruption curve. Subglacial eruptions are supported equally by assimilation or by loading of the crust by ice. Applied to HMV, the implications are that phonolite magmas can be erupted without ice loading given sufficient AFC (*F*=68%). However, the accumulation of ice can be used to tap less contaminated, denser magmas.

The region between the two solid curves (B) establishes a wide range of compositional and environmental conditions that would support subglacial to supraglacial eruptions of HMV magmas. Taken together, these two curves suggest that ice loading and unloading above crustal magma chambers could explain the style and episodic nature of magmatism recorded by Hoodoo Mountain volcano.

Conclusions

Hoodoo Mountain volcano formed over a protracted period of time and reflects a complex combination of physical and chemical processes. Abundant field, stratigraphic and morphologic evidence attests to substantial interactions between volcanism and large ice masses at least four times during the 100-ka eruptive history of HMV. The lack of significant chemical and mineralogical variability over this same time period argues for the sustained production of evolved magma of nearly uniform composition. A combination of fractional crystallization of alkaline basaltic magma coupled with assimilation of crustal rocks can produce sufficient volumes of low density, phonolite magma to form HMV. The postulated AFC processes produce derivative magmas with densities low enough to produce the subglacial eruptions documented throughout the HMV stratigraphy. The combination of AFC processes and fluctuations in local ice thickness since 100 ka produce a coherent model for explaining the episodic eruptions from HMV.

Acknowledgements This research was supported by the Geological Survey of Canada through the Iskut Field Mapping Program (RGA) and the NSERC Research Grants program (89820 to J.K.R.). The senior author was supported by the University of British Columbia through a University Graduate Fellowship (1995–1997). Our research benefited from discussions with J. Nicholls, C. Hickson, and M. Stasiuk, who we thank for critically reading earlier versions of the manuscript. Our arguments were greatly clarified during the review process and we thank T. Feeley, H. Tuffen, and W. Hildreth for their thorough and constructive reviews.

References

Allen CC, Jercinovic MJ, Allen JSB (1982) Subglacial volcanism in north-central British Columbia and Iceland. J Geol 90: 699–715

Anderson RG (1993) A Mesozoic stratigraphic and plutonic framework for northwestern Stikinia (Iskut River area), northwestern British Columbia, Canada. In: Dunne G, McDougall K (eds)Mesozoic paleogeography of the western United States, vol II.. Society of Economic Paleontology and Mineralogy. Pacific Section no 71, pp 477–494

Bergh SG, Sigvaldason GE (1991) Pleistocene mass-flow deposits of basaltic hyaloclastite on a shallow submarine shelf, South Iceland. Bull Volcanol 53:597–611

Carignan J, Ludden J, Francis D (1994) Isotopic characteristics of mantle sources for Quaternary continental alkaline magmas in the northern Canadian Cordillera. Earth Planet Sci Lett 128:271–286

Cousens BL, Bevier ML (1995) Discerning asthenospheric, lithospheric and crustal influences on the geochemistry of Quaternary basalts from the Iskut–Unuk rivers area, northwestern British Columbia. Can J Earth Sci 32:1451–1461

DeGraff JM, Aydin A (1993) Effects of thermal regime on growth increment and spacing of contraction joints in basaltic lava. J Geophys Res 98:6411–6430

Dixon JE, Filiberto JR, Moore JG, Hickson CJ (2002) Volatiles in basaltic glasses from a subglacial volcano in northern British Columbia: implications for mantle volatiles and ice sheet thickness. In: Smellie J (ed) Volcano–ice interactions. Geol Soc Lond Spec Publ (in press)

Edwards BR (1997) Field, kinetic and thermodynamic studies of magmatic assimilation in the northern Cordilleran volcanic province, northwestern British Columbia. PhD Thesis, University of British Columbia

Edwards BR, Russell JK (1996) Influence of magmatic assimilation on mineral growth and zoning. Can Mineral 34:1149–1162

Edwards BR, Russell JK (1998) Time scales of magmatic processes: new insights from dynamic models for magmatic assimilation. Geology 26:1103–1106

Edwards BR, Russell JK (1999) Northern Cordilleran volcanic province: a northern basin and range? Geology 27:243–246

Edwards BR, Russell JK (2000) Distribution, nature and origin of Neogene–Quaternary magmatism in the northern Cordilleran volcanic province, Canada. Geol Soc Am Bull 112:1280–1295

Edwards BR, Russell JK, Anderson RG, Villeneuve M, Hastings N (1999) Punctuated, peralkaline, subglacial volcanism at Hoodoo Mountain volcano, northwestern British Columbia, Canada. Am Geophys Union, Fall Meeting, San Francisco, CA, V12A-02

Edwards BR, Anderson RG, Russell JK, Hastings NL, Guo YT (2000) The Quaternary Hoodoo Mountain Volcanic Complex and Paleozoic and Mesozoic basement rocks, parts of Hoodoo Mountain (NTS 104B/14) and Craig River (NTS 104B/11) map areas, northwestern British Columbia. Geological Survey of Canada, Open File Map 3721, 1:20,000 scale

Eiché GE, Francis DM, Ludden JN, (1987) Primary alkaline magmas associated with the Quaternary Alligator lake volcanic complex, Yukon Territory, Canada. Contrib Mineral Petrol 95: 191–201

Foster HL, Forbes RB, Ragan DM (1966) Granulite and peridotite inclusions from Prindle Volcano, Yukon–Tanana Upland, Alaska. US Geol Survey Professional Paper 1966, pp B115–B119

Francis D, Ludden J (1990) The mantle source for olivine nephelinite, basanite and alkaline olivine basalts at Fort Selkirk, Yukon, Canada. J Petrol 31:371–400

Fudali RF (1963) Experimental studies bearing on the origin of pseudoleucite and associated problems of alkalic rock systems. Geol Soc Am Bull 74:1101–1125

Furnes H, Fridleifsson IB, Atkins FB (1980) Subglacial hyaloclastites – on the formation of acid hyaloclastites. J Volcanol Geotherm Res 8:95–110

Ghiorso MS, Sack RO (1995) Chemical mass transfer in magmatic processes. IV. A revised and internally-consistent thermodynamic model for the interpolation and extrapolation of liquid-solid equilibria in magmatic systems at elevated temperatures and pressures. Contrib Mineral Petrol 119:197–212

Grove EW (1974) Deglaciation – a possible triggering mechanism for Recent volcanism. International Association of Volcanology and Chemistry of the Earth's Interior, Proceedings of the Symposium on Andean and Antarctic Volcanology Problems, Santiago, Chile, September 1974, pp 88–97

Hamilton TS (1981) Late Cenozoic alkaline volcanics of the Level Mountain Range, northwestern British Columbia: geology, petrology, and paleomagnetism. PhD Thesis, The University of Alberta, Edmonton

Hammer PTC, Clowes RM (2000) Lithospheric structure across the Coast orogen of NW British Columbia and SE Alaska from seismic wide-angle studies: lithoprobe SNORE Line 22 and ACCRETE profiles, in SNORCLE Transect and Cordilleran Tectonics Workshop Meeting. Lithoprobe Report No. 72, compiled by Cook F, Erdmer P, pp 218–223

Hammer PTC, Clowes RM, Ellis RM (2000) Crustal structure of NW British Columbia and SE Alaska from seismic wide-angle studies: coast plutonic complex to Stikinia. J Geophys Res 105:7961–7981

Hauksdóttir S, Enegren EG, Russell JK (1994) Recent basaltic volcanism in the Iskut–Unuk rivers area, northwestern BC. In: Current research, part A, geological survey of Canada, paper 1994-1A. Geological Survey of Canada, Ottawa, Ontario, pp 57–67

Hay DE, Wendlandt RF (1995) The origin of Kenya Rift plateau–type flood phonolites; results of high-pressure/high-pressure experiments in the systems phonolite–H_2O and phonolite–H_2O–CO_2. J Geophys Res 100:401–410

Hickson CJ (1991) Volcano vent map and table. In: Wood CA, Kienle J (eds) Volcanoes of North America. Cambridge University Press, New York, pp 116–118

Hickson CJ (2000) Physical controls and resulting morphological forms of Quaternary ice-contact volcanoes in western Canada. Geomorphology 32:239–261

Hyndman R, Lewis T (1999) Geophysical consequences of the Cordillera–Craton thermal transition in southwestern Canada. Tectonophysics 306:397–422

Irvine TN, Baragar WRA (1971) A guide to the chemical classification of the common volcanic rocks. Can J Earth Sci 8:523–548

Kaszuba JP, Wendlandt RF (2000) Effect of carbon dioxide on dehydration melting reactions and melt compositions in the lower crust and the origin of alkaline rocks. J Petrol 41:363–386

Kerr FA (1948) Lower Stikine and western Iskut River areas. Geol Surv Can Memoir 248

Kuntzmann T, Blasse UW (2000) The differentiation of tephritic melt: an experimental study. American Geophysical Union Transepts, Fall Meeting

Kyle PR, Moore JA, Thirlwall MF (1992) Petrologic evolution of anorthoclase phonolite lavas at Mount Erebus, Ross Island, Antarctica. J Petrol 33:849–875

LeBas MJ, LeMaitre RW, Streckeisen A, Zanettin B (1986) A chemical classification of volcanic rocks based on the total alkali–silica diagram. J Petrol 27:745–750

LeMaitre RW (1989) A classification of igneous rocks and glossary of terms. Blackwell, Oxford

Le Roex AP, Cliff RA, Adair BJI (1990) Tristan da Cunha, South Atlantic; geochemistry and petrogenesis of a basanite–phonolite lava series. J Petrol 31:779–812

Lescinsky DT, Fink JH (2000) Lava and ice interactions at stratovolcanoes: use of characteristic features to determine past glacial extents and future volcanic hazards. J Geophys Res 105:23711–23726

Long PE, Wood BJ (1986) Structures, textures, and cooling histories of Columbia River basalt flows. Geol Soc Am Bull 97:1144–1155

Mathews WH (1947) Tuyas, flat-topped volcanoes in northern British Columbia. Am J Sci 245:560–570

McDonough WF, Sun SS (1995) The composition of the earth. Chem Geol 120:223–253

Peltier WR (1994) Ice age paleotopography. Science 265:195–201

Rampino MR, Self S, Fairbridge RW (1979) Can rapid climatic changes cause volcanic eruption? Science 206:826–828

Russell JK, Hauksdóttir S (2000) Estimates of crustal assimilation in Quaternary lavas from the northern Cordillera, British Columbia. Can Mineral 39:275–297

Russell JK, Stasiuk MV, Page T, Nicholls J, Rust A, Cross G, Schmok J, Edwards BR, Hickson, CJ, Maxwell M (1998) Radar studies of the Hoodoo icecap, Iskut River region, British Columbia. In: Current research, part A; Geological Society of Canada paper 98-1A, Otawa, Ontario, pp 55–63

Sigvaldason GE, Annertz K, Nilsson M (1992) Effects of glacier loading/deloading on volcanism: postglacial volcanic production rate of the Dyngjufjoll area, central Iceland. Bull Volcanol 54:385–392

Skilling IP (1994) Evolution of an englacial volcano: Brown Bluff, Antarctica. Bull Volcanol 56:573–591

Smellie JL (1999) Subglacial eruptions. In: Sigurdsson H (ed) Encyclopedia of volcanoes. Academic Press, San Diego, pp 403–418

Smellie JL, Hole MJ (1997) Products and processes in Pliocene–Recent, subaqueous to emergent volcanism in the Antarctic Peninsula: examples of englacial Surtseyan volcano construction. Bull Volcanol 58:628–646

Smellie JL, Skilling IP (1994) Products of subglacial volcanic eruptions under different ice thicknesses: two examples from Antarctica. Sediment Geol 91:115–129

Souther JG (1977) Volcanism and tectonic environments in the Canadian Cordillera – a second look. In: Baragar WRA, Coleman LC, Hall JM (eds) Volcanic regimes in Canada. Geol Assoc Can Spec Pap 16:3–24

Souther JG (1991a) Hoodoo Mountain: In: Wood CA, Kienle J (eds) Volcanoes of North America, United States and Canada. Cambridge University Press, Cambridge, pp 127–128

Souther JG (1991b) Iskut–Unuk River Cones, Canada. In: Wood CA, Kienle J (eds) Volcanoes of North America, United States and Canada. Cambridge University Press, pp 128–129

Souther JG (1992) The late Cenozoic Mount Edziza Volcanic Complex, British Columbia. Geological Survey of Canada Memoir 420

Souther JG, Hickson CJ (1984) Crystal fractionation of the basalt comendite series of the Mount Edziza volcanic complex, British Columbia: major and trace elements. J Volcanol Geotherm Res 21:79–106

Souther JG, Armstrong RL, Harakal J (1984) Chronology of the peralkaline, late Cenozoic Mount Edziza volcanic complex, northern British Columbia. Geol Soc Am Bull 95:337–349

Stasiuk M, Russell JK (1989) Quaternary volcanic rocks of the Iskut River region, northwestern British Columbia. Current research, part E. Geological Survey of Canada, Paper 1990-1E, Ottawa, Ontario, pp 153–157

Stumpf AJ, Broster BE, Levson VM (2000) Multiphase flow of the late Wisconsinan cordilleran ice sheet in western Canada. Geol Soc Am Bull 112:1850–1863

Trupia S, Nicholls J (1996) Petrology of Recent lava flows, Volcano Mountain, Yukon Territory, Canada. Lithos 37:61–78

Tuffen H, Gilbert J, McGarvie D (2001) Products of an effusive subglacial rhyolite eruption: Blahnukur, Torfajokull, Iceland. Bull Volcanol 63:179–190

Villeneuve ME, Whalen JB, Edwards BR, Anderson RG (1998) Time-scales of episodic magmatism in the Canadian Cordillera as determined by ^{40}Ar–^{39}Ar geochronology. GAC-MAC 1998 Annual Meeting Program with Abstracts, Quebec City, A192

Watson KDP, Mathews WH (1948) Partly vitrified xenoliths in pillow basalt (British Columbia). Am J Sci 246:601–614

Werner R, Schmincke H-U (1999) Englacial vs. lacustrine origin of volcanic table mountains: evidence from Iceland. Bull Volcanol 60:335–354

Wilson M, Downes H, Cebria J-M (1995) Contrasting fractionation trends in coexisting continental alkaline magma series; Cantal, Massif Central, France. J Petrol 36:1729–1753